

1-1-2020

Fe-based metallic glasses and dyes in fenton-like processes: Understanding their intrinsic correlation

Xueqing Wang

Edith Cowan University, xueqing.wang@ecu.edu.au

Qiaoyue Zhang

Edith Cowan University, qiaoyuez@our.ecu.edu.au

Shun-Xing Liang

Edith Cowan University, s.liang@ecu.edu.au

Zhe Jia

Wenchang Zhang

See next page for additional authors

Follow this and additional works at: <https://ro.ecu.edu.au/ecuworkspost2013>



Part of the [Engineering Commons](#)

[10.3390/catal10010048](https://doi.org/10.3390/catal10010048)

Wang, X., Zhang, Q., Liang, S. X., Jia, Z., Zhang, W., Wang, W., & Zhang, L. C. (2020). Fe-based metallic glasses and dyes in fenton-like processes: Understanding their intrinsic correlation. *Catalysts*, *10*(1), 48. <https://doi.org/10.3390/catal10010048>

[10.3390/catal10010048](https://doi.org/10.3390/catal10010048)

This Journal Article is posted at Research Online.




<https://ro.ecu.edu.au/ecuworkspost2013/7518>

Authors

Xueqing Wang, Qiaoyue Zhang, Shun-Xing Liang, Zhe Jia, Wenchang Zhang, Weimin Wang, and Lai-Chang Zhang

Article

Fe-Based Metallic Glasses and Dyes in Fenton-Like Processes: Understanding Their Intrinsic Correlation

Xueqing Wang ¹, Qiaoyue Zhang ¹, Shun-Xing Liang ^{1,*}, Zhe Jia ², Wenchang Zhang ³,
Weimin Wang ^{4,*} and Lai-Chang Zhang ^{1,*}

¹ School of Engineering, Edith Cowan University, 270 Joondalup Drive, Joondalup, Perth, WA 6027, Australia; xwang29@our.ecu.edu.au (X.W.); qiaoyuez@our.ecu.edu.au (Q.Z.)

² School of Mechanical and Manufacturing Engineering, UNSW Sydney, Sydney, NSW 2052, Australia; zhe.jia2@unsw.edu.au

³ Ji'an Ecological Environment Monitoring Center of Jiangxi Province, Ji'an 343000, Jiangxi, China; domingozhang@163.com

⁴ School of Materials Science and Engineering, Shandong University, Jinan 250061, Shandong, China

* Correspondence: sxliang90@gmail.com (S.-X.L.); weiminw@sdu.edu.cn (W.W.); lczhangimr@gmail.com or l.zhang@ecu.edu.au (L.-C.Z.)

Received: 3 December 2019; Accepted: 17 December 2019; Published: 1 January 2020



Abstract: Fe-based metallic glasses have been demonstrated as effective heterogeneous catalysts in Fenton-like processes for dye degradation. Yet, currently corresponding studies have limitations due to the limited study object (dyes) and the correlation between metallic glasses and dye pollutants in Fenton-like processes is still not comprehensively studied. Accordingly, this work intensively investigated the thermal catalytic behavior correlations between two Fe-based metallic glasses ($\text{Fe}_{78}\text{Si}_9\text{B}_{13}$ and $\text{Fe}_{73.5}\text{Si}_{13.5}\text{B}_9\text{Cu}_1\text{Nb}_3$) and eight different dyes. Results indicated a lower activation energy in the more active metallic glass and a dependence of the activation energy of Fe-based metallic glasses in dye solutions. In addition, a high H_2O_2 concentration led to a declined catalytic efficiency but a photo-enhanced Fenton-like process overcame this limitation at high concentration of H_2O_2 due to the decrease of pH and enhancement of irradiation. Furthermore, the average mineralization rates of $\text{Fe}_{78}\text{Si}_9\text{B}_{13}$ and $\text{Fe}_{73.5}\text{Si}_{13.5}\text{B}_9\text{Cu}_1\text{Nb}_3$ have been measured to be 42.7% and 12.6%, respectively, and the correlation between decolorization and mineralization revealed that a faster decolorization in a Fenton-like process contributed to a higher mineralization rate. This work provides an intrinsic viewpoint of the correlation between Fe-based metallic glasses and dyes in Fenton-like processes and holds the promise to further promote the industrial value of metallic glasses.

Keywords: metallic glasses; dyes; Fenton-like processes; activation energy; mineralization

1. Introduction

In recent years, metallic glasses with long-range disordered atomic configurations have been extensively investigated as novel functional catalysts in environmental and energy science [1–4]. Compared to catalysts with highly ordered crystalline structures, their uniquely amorphous structures fabricated by rapid solidification processes endow metallic glasses with many fascinating catalytic properties, such as high surface active sites induced by unsaturated coordination of atomic numbers [5], fast electron transfer [6], low thermal activation energy barriers [7], self-stabilizing nature [8] and structural stability [9,10]. Particularly, low-cost Fe-based metallic glasses with their easily modified chemical composition, good glass-forming ability and environmentally friendly nature have attracted increasing interest as catalysts in renewable energy conversion. For example, $\text{Fe}_{40}\text{Co}_{40}\text{Se}_{20}$ supported on carbon fiber paper [11], $\text{Fe}_{40}\text{Ni}_{40}\text{P}_{20}$ [5,12] and $\text{Fe}_{40}\text{Co}_{40}\text{P}_{13}\text{C}_7$ [13] metallic glass ribbons were directly

employed as electrocatalysts for efficient hydrogen/oxygen evolution reactions; a comparative study between metallic glasses and their crystalline counterparts also suggests that the amorphous structure easily induces a much higher active catalytic activity [12] and the functionality of amorphous structures with active sites and reduced energy barriers has been demonstrated [14]. Recently, stimulated by global environmental pressure, the attractive catalytic properties in Fe-based metallic glasses have become tremendous advantages for the treatment of environmental pollutants [15].

Advanced oxidation processes (AOPs) have been considered as effective methods to purify organic contaminants [16], which cannot be achieved by conventional chemical, physical and biological methods [17–20]. The major contribution to effective pollutant degradation from AOPs is usually attributed to the formation of reactive species with high redox potential, such as hydroxyl radical ($\bullet\text{OH}$, $E^0 = 2.7\text{ V}$) [21]. Fenton/Fenton-like processes are one type of effective AOPs to generate $\bullet\text{OH}$ by hydrogen peroxide (H_2O_2) and iron-containing materials under acidic conditions. Given the fact that the amorphous nature facilitates Fe-based metallic glasses to have better catalytic properties than crystalline catalysts, they have been applied as a superior alternative of crystalline iron catalysts in Fenton-like processes. It has been reported that $\text{Fe}_{78}\text{Si}_9\text{Si}_{13}$ metallic glass ribbons presented 5–10 times faster of $\bullet\text{OH}$ production rate than other Fe-based crystalline catalysts in methylene blue and methyl orange dye degradation [22]; $\text{Fe}_{50}\text{Ni}_{30}\text{P}_{13}\text{C}_7$ metallic glass ribbons displayed a 2-fold enhanced catalytic efficiency by surface reactivation in a Fenton-like process [23]; $\text{Fe}_{80}\text{P}_{13}\text{C}_7$ metallic glass ribbons showed self-renewing and ultra-strong catalytic reusability in dye decomposition [24,25]. Very recently, our research group has also demonstrated that $\text{Fe}_{78}\text{Si}_9\text{B}_{13}$ metallic glass ribbons could be effective environmental catalysts not only for the aforementioned degradation of organic pollutants, but also for remediation of inorganic pollutants (arsenic and nitrate) [26], showing a high promise of industrial value.

Due to the development of economy and the increased demand of market, synthetic dyes are currently widely applied in many industries, especially in the textile industry as coloring agents [27]. According to their chemical structures and functional groups, dyes with chromophore and auxochrome groups are classified into azo dyes, triarylmethane dyes, xanthene dyes, etc. [28]. Chromophore groups determine the presence of color by absorbing light within the visible spectrum while auxochrome groups determine the color intensity [29]. Functional groups such as amino, hydroxyl, nitro and carbonyl groups can further alter the light absorbance capability of chromophore groups [30]. However, dye molecules not only contain genotoxic and carcinogenic substances but also have chemically stable structures of a recalcitrant nature [31], which will cause detrimental effects on the aquatic environment if a dye solution is discharged without effective treatment. In addition, the synthesis methods of dyes make their chemical structures more and more complicated, which also greatly increases the difficulty for degrading dyes into harmless substances. It is thus urgent to identify and exploit effective methods to alleviate the environmental pressure.

Although Fe-based metallic glasses used in Fenton-like processes have been investigated for effective dye degradation in recent years, these studies mostly focused on specific dye degradation leading to a significant limitation. In addition, the correlation between metallic glasses and dyes is not yet fully understood. Therefore, motivated by these limitations, our research group focused on two Fe-based metallic glasses ($\text{Fe}_{78}\text{Si}_9\text{B}_{13}$ and $\text{Fe}_{73.5}\text{Si}_{13.5}\text{B}_9\text{Cu}_1\text{Nb}_3$) in Fenton-like processes to degrade eight dyes with different classifications (i.e., azo dyes, thiazine dye, triarylmethane dyes and nitroso dye), aiming to understand the intrinsic correlation of Fe-based metallic glasses and dyes in Fenton-like processes.

2. Results and Discussion

2.1. Dye Characteristics and Properties

The ultraviolet (UV)-visible (Vis) spectra of the eight different dyes are shown in Figure 1. In order to distinguish the functional groups in their chemical structures, the UV-Vis spectra have been divided

into the Vis and UV region (Figure 1a,b, respectively). As shown in Figure 1a, the intensities and absorbance peaks of different dyes with the same concentration (20 ppm) are apparently different, where the peak intensity of methylene blue (MB) is stronger than that of the other dyes. Cibacron brilliant yellow 3G-P (BY), cibacron brilliant red 3B-A (BR) and naphthol green B (NG) dyes have the lowest peak intensity among all eight dyes. According to the characteristic peaks of dyes in the Vis spectra, Table 1 summarizes their absorbance peak positions (λ_{max}), which generally dominate the reflection of their colors by light absorbance. In addition, all the dye structures are shown in Table 1, where their functional groups and state of charge are clearly indicated for their classification. Accordingly, methyl orange (MO), bright black BN (BB), BY and BR dyes can be classified as azo dyes due to the presence of a nitrogen double bond ($-N=N-$) functional group with an anionic charge and they have been widely studied in recent years [22,32–34]. MB dye with a four-carbon ring, one nitrogen and one sulfur atom is classified as a thiazine dye and it is commonly used in medications [24,35]. Nowadays many researchers tend to employ MB dye as a classical organic pollutant example, since it is relatively stable at different pH values and solution temperatures, so as to investigate effect of AOPs using different catalysts [9,36–38]. With triphenylmethane backbones, both crystal violet (CV) and malachite green (MG) dyes can be grouped as triarylmethane dyes with cationic charges and usually present intense color [39]. It should be noted that MG dye has a self-conversion between the MG molecule and MG leucocarinol [40]. NG dye with a $-N=O$ functional group can be classified as a nitroso dye.

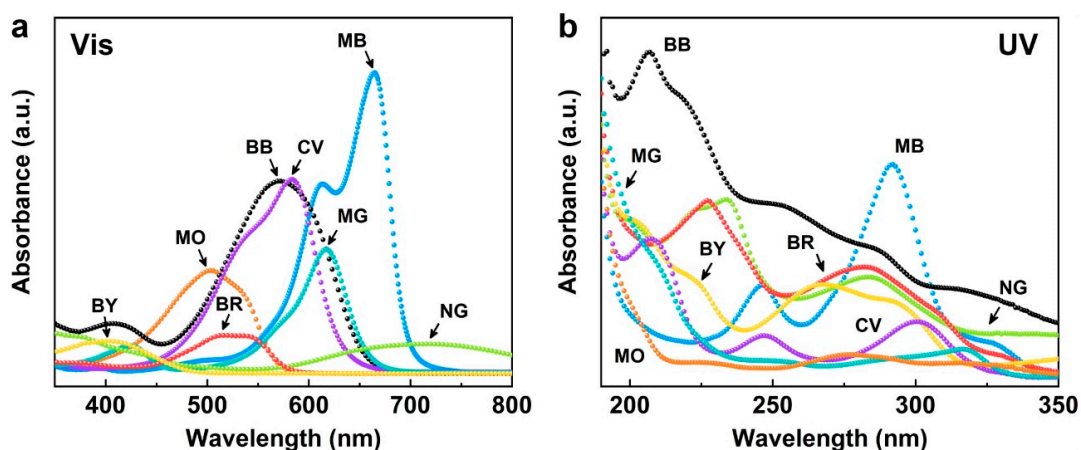
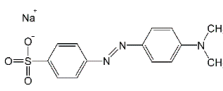
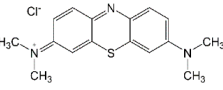
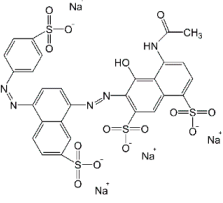
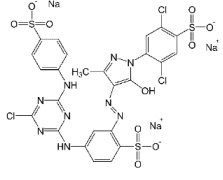
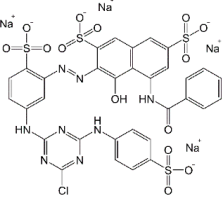
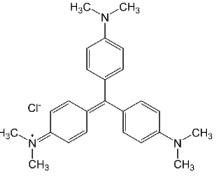
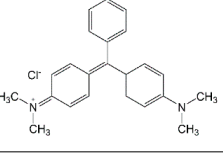
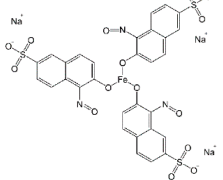


Figure 1. (a) Visible spectra of eight dyes (i.e., MO, MB, BB, BY, BR, CV, MG and NG) as organic pollutants ($[Dye]_0 = 20$ ppm, pH = 3.0). (b) Corresponding ultraviolet spectra of the eight dyes under the same conditions.

It should be mentioned that in addition to chromophore groups, most dye molecules are attached to benzene rings or/and heterocyclic aromatic molecules, leading to additional absorbance peaks located at the UV region of UV-Vis spectra, as demonstrated in Figure 1b. All the dye absorbance spectra in the UV region contain more than one peak, indicating that the intrinsic aromatic structures are more complicated than just the chromophore groups. It is also interesting to find that some azo dyes (e.g., BR and BY) with a large molecular weight and a low peak intensity in the Vis region, however, have a high peak intensity in the UV region. In contrast, the peak intensities of triarylmethane dyes (i.e., CV and MG) in the UV region are relatively lower than the peaks in the Vis region. Although hydroxyl radicals ($\bullet OH$) produced by Fenton-like processes have strong and non-selective oxidation properties towards organic pollutants [41], the intrinsically distinguishable chemical structures of dyes in fact may lead to side reactions during their degradation, and the degradation effect of dyes may be even closely related to the type of catalysts used, which is still not fully understood in the Fenton-like processes catalyzed by Fe-based metallic glasses.

Table 1. Characteristics of the dyes.

Dye	Classification	Empirical Formula	Molecular Weight (g/mol)	λ_{\max} (nm)	Structure	Ref.
Methyl Orange (MO)	Azo-anionic	$C_{14}H_{14}N_3NaO_3S$	327.33	498		[9,22,42]
Methylene Blue (MB)	Thiazine-cationic	$C_{16}H_{18}ClN_3S$	319.85	664		[24,43–45]
Bright Black BN (BB)	Azo-anionic	$C_{28}H_{17}N_5Na_4O_{14}S_4$	867.68	570		[23]
Cibacron Brilliant Yellow 3G-P (BY)	Azo-anionic	$C_{25}H_{19}Cl_3N_9Na_4O_{10}S_3$	831.02	404		[46]
Cibacron Brilliant Red 3B-A (BR)	Azo-anionic	$C_{32}H_{24}ClN_8Na_4O_{14}S_4$	1000.25	517		[33,47]
Crystal Violet (CV)	Triarylmethane-cationic	$C_{25}N_3H_{30}Cl$	407.98	582		[16,48]
Malachite Green (MG)	Triarylmethane-cationic	$C_{23}H_{25}ClN_2$	364.91	618		[27,40,49]
Naphthol Green B (NG)	Nitroso-anionic	$C_{30}H_{15}FeN_3Na_3O_{15}S_3$	878.45	714		[50]

2.2. Thermal Catalytic Behavior Correlation Between Metallic Glasses and Dyes

Generally, the intrinsic activation of chemical reaction by catalysts may have various behaviors and the thermal activation energy barrier (ΔE) is commonly used to investigate the thermal behavior of catalysts in their reactions. Many studies have demonstrated that metallic glasses as amorphous catalysts have lower ΔE than most crystalline alloy catalysts, indicating that the amorphous nature of

the catalysts facilitates the occurrence of degradation processes [7,51,52]. The ΔE of metallic glasses are generally lower than 60 kJ/mol [9]. However, this fact does not indicate that the ΔE of the same metallic glass will be constant toward reactions in the different dyes since the reaction temperature environment may also affect degradation of dye with variation of structure so as to influence the whole process of degradation by the metallic glass, which is not fully understood. As such, $\text{Fe}_{78}\text{Si}_9\text{B}_{13}$ and $\text{Fe}_{73.5}\text{Si}_{13.5}\text{B}_9\text{Cu}_1\text{Nb}_3$ metallic glass ribbons have been employed to investigate their thermal catalytic behavior with the eight different dyes. In this work, the ΔE of specific metallic glass ribbons with dyes is measured from the corresponding first-order reaction rate constant (k) under reaction temperatures of 25, 30, 35 and 40 °C. The ΔE is obtained by the Arrhenius equation: $\ln k_{\text{obs}} = -\Delta E/RT + \ln A$, where k is first-order reaction rate constant, R is the gas constant (8.314 J/(mol·K)), T is the absolute temperature (K), and A is a pre-exponential factor.

Figure 2a–h show the degradation performance of $\text{Fe}_{78}\text{Si}_9\text{B}_{13}$ metallic glass ribbons on the eight different dyes from 25 to 40 °C. It can be seen that almost all the dye decolorizations reach completion within 10 min at 25 °C, showing the outstanding catalytic performance of $\text{Fe}_{78}\text{Si}_9\text{B}_{13}$ metallic glass ribbons in the Fenton-like process due to their fast electron transfer ability and relatively strong surface stability, which have been intrinsically investigated in recent years [6,9]. However, two dyes (BY and NG) present exceptional decolorization performance, where BY reaches a 90% decolorization and the NG decolorization rate is about 80% within 10 min at the same temperature (25 °C). In addition, compared to our previous work [50], the NG decolorization rate in the Fenton-like process in this work is slightly lower than that in the photo-enhanced sulfate radical-based AOPs (about 95%) in previous work using the same $\text{Fe}_{78}\text{Si}_9\text{B}_{13}$ metallic glass ribbons. The higher decolorization rate of NG in the photo-enhanced sulfate radical-based AOPs may be attributed to the effect of the external UV-Vis irradiation effect and the different AOPs system used. Both BY and NG show negligible enhancement effect upon full completion of dye decolorization although the reaction rate is enhanced at high temperatures. This enhanced reaction rate has also been observed in the other six dyes (MO, MB, BB, BR, CV and MG) when the reaction temperature is increased. In fact, the temperature also has a similar effect as UV-Vis irradiation, which facilitates completion of faster reactions due to the supplementary activation by the external energy [33].

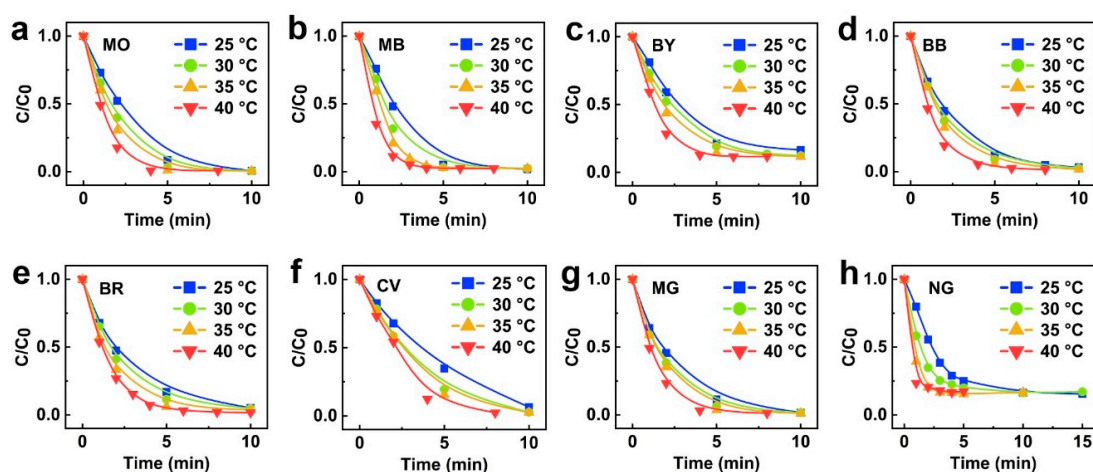


Figure 2. Decolorization of (a) MO, (b) MB, (c) BY, (d) BB, (e) BR, (f) CV, (g) MG and (h) NG by $\text{Fe}_{78}\text{Si}_9\text{B}_{13}$ metallic glass ribbons under 25–40 °C without UV-Vis irradiation (dye concentration: 20 ppm, catalyst dosage: 0.5 g/L, H_2O_2 concentration: 1 mM, pH 3.0). Decolorization rates were measured from the λ_{max} of corresponding UV-Vis spectra with reaction time.

On the other hand, the decolorization behaviors of $\text{Fe}_{73.5}\text{Si}_{13.5}\text{B}_9\text{Cu}_1\text{Nb}_3$ metallic glass ribbons against the dyes at 25 to 40 °C are shown in Figure 3a–h. The decolorization efficiencies of $\text{Fe}_{73.5}\text{Si}_{13.5}\text{B}_9\text{Cu}_1\text{Nb}_3$ are apparently lower than those of $\text{Fe}_{78}\text{Si}_9\text{B}_{13}$ seen in Figure 2 due to the lower

surface adsorption ability and stronger surface protection in $\text{Fe}_{73.5}\text{Si}_{13.5}\text{B}_9\text{Cu}_1\text{Nb}_3$ [22,47]. The inclusion of Cu and Nb will also contribute to a lower electron transfer ability [53]. In this work, most of dye decolorization by $\text{Fe}_{73.5}\text{Si}_{13.5}\text{B}_9\text{Cu}_1\text{Nb}_3$ reached completion within 60 min and the decolorization rates also increase with the reaction temperatures. However, the decolorization of the two triarylmethane dyes (CV and MG) seemed to be inhibited when using $\text{Fe}_{73.5}\text{Si}_{13.5}\text{B}_9\text{Cu}_1\text{Nb}_3$ as a catalyst (Figure 3f,g). In particular, CV dye can only be decolorized by less than 40% within 45 min and under 40 °C. The CV and MG dye molecules have the same cationic charge in solution, which makes them different from the other dye molecules with anionic charges. It should be noted that the decolorization performance of $\text{Fe}_{73.5}\text{Si}_{13.5}\text{B}_9\text{Cu}_1\text{Nb}_3$ on the cationic dye MB does not show any inhibitory behavior, which may be attributed to a combination of the thiazine dye structure and a molecular charge favorable to the degradation in Fenton-like processes by Fe-based metallic glasses. The inhibited decolorization in CV and MG is possibly attributed to their triarylmethane structures when Cu or/and Nb are present in metallic glasses. In fact, the molecule charge affects the dye absorption on the ribbon surface and further affects the degradation during the processes. Considering the aforementioned catalytic degradation of both two metallic glass ribbons in Figures 2 and 3, the decolorization of dyes in Fenton-like processes can be affected by their molecular charge, and dye and catalyst structures.

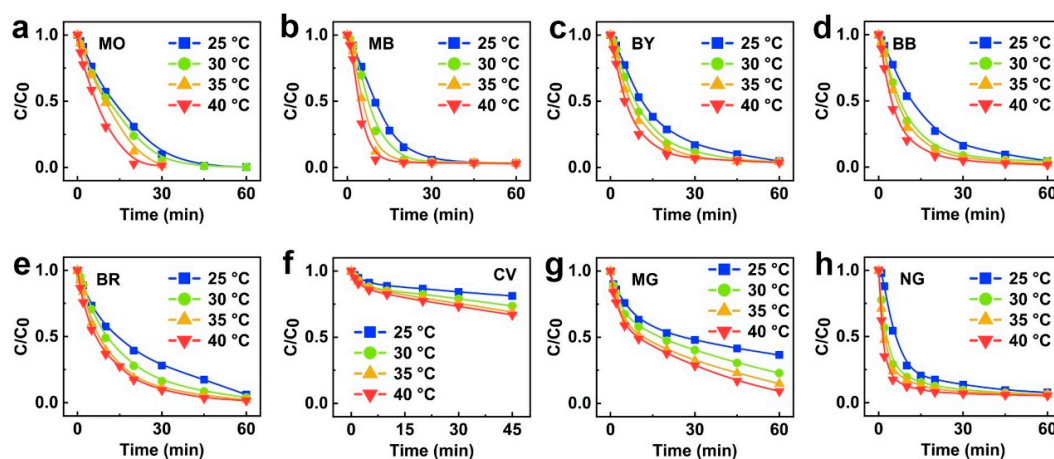


Figure 3. Decolorization of (a) MO, (b) MB, (c) BY, (d) BB, (e) BR, (f) CV, (g) MG and (h) NG by $\text{Fe}_{73.5}\text{Si}_{13.5}\text{B}_9\text{Cu}_1\text{Nb}_3$ metallic glass ribbons under 25–40 °C without UV-Vis irradiation (dye concentration: 20 ppm, catalyst dosage: 0.5 g/L, H_2O_2 concentration: 1 mM, pH 3.0). Decolorization rates were measured from the λ_{max} of the corresponding UV-Vis spectra with reaction time.

Accordingly, the reaction rate constants for different reaction temperatures measured from Figures 2 and 3 have been summarized in Table 2. In addition to the Arrhenius equation, all the ΔE for different dyes can be obtained by the slope of fitting curve of $-\ln k$ as a function of $1000/RT$. As shown in Figure 4, the fitting of Arrhenius curve is classified by used dyes and all the obtained ΔE values have been shown based on metallic glass ribbons. It should be noted that the fitting of NG dye using $\text{Fe}_{78}\text{Si}_9\text{B}_{13}$ only includes 25–35 °C due to the extremely fast decolorization at 40 °C. In order to make it clearer, Figure 5 summarizes all the ΔE values according to dyes and metallic glass ribbons. It is clear that ΔE of $\text{Fe}_{73.5}\text{Si}_{13.5}\text{B}_9\text{Cu}_1\text{Nb}_3$ is always higher than that of $\text{Fe}_{78}\text{Si}_9\text{B}_{13}$, confirming that $\text{Fe}_{78}\text{Si}_9\text{B}_{13}$ metallic glass ribbons are always easier to activate than $\text{Fe}_{73.5}\text{Si}_{13.5}\text{B}_9\text{Cu}_1\text{Nb}_3$ in a Fenton-like process. A range of ~10–30 kJ/mol of ΔE of difference between $\text{Fe}_{78}\text{Si}_9\text{B}_{13}$ and $\text{Fe}_{73.5}\text{Si}_{13.5}\text{B}_9\text{Cu}_1\text{Nb}_3$ can be estimated from Figure 5. In BR dye, ΔE presents the closest value for the two metallic glasses and MB dye shows the biggest difference. However, ΔE of the same metallic glass in the degradation of different dyes varies, indicating that ΔE of a metallic glass also depends on the reaction environment (dyes in this work) and it is not always consistent for the same material. This fact also indicates that any comparison of ΔE values for different catalysts should also consider if the reaction environment is consistent.

Table 2. Reaction rate constants (k) of dye degradation by $\text{Fe}_7\text{Si}_9\text{B}_{13}$ and $\text{Fe}_{73.5}\text{Si}_{13.5}\text{B}_9\text{Cu}_1\text{Nb}_3$ metallic glass ribbons under different reaction temperatures. All the k values were obtained from Figures 2 and 3 with fixed catalyst dosage (0.5 g/L).

Catalyst	Reaction Temperature (°C)	Dye Reaction Rate Constant k (min^{-1})							
		MO	MB	BY	BB	BR	CV	MG	NG
$\text{Fe}_7\text{Si}_9\text{B}_{13}$	25	0.548	0.692	0.336	0.377	0.346	0.285	0.413	0.341
	30	0.711	0.760	0.335	0.487	0.430	0.352	0.569	0.416
	35	1.070	0.856	0.386	0.588	0.560	0.407	0.709	0.434
	40	1.410	0.961	0.494	0.709	0.662	0.455	0.931	-
$\text{Fe}_{73.5}\text{Si}_{13.5}\text{B}_9\text{Cu}_1\text{Nb}_3$	25	0.061	0.099	0.051	0.051	0.038	0.003	0.010	0.022
	30	0.074	0.152	0.066	0.085	0.055	0.004	0.018	0.026
	35	0.120	0.235	0.088	0.110	0.065	0.006	0.025	0.036
	40	0.211	0.313	0.118	0.128	0.090	0.007	0.033	0.051

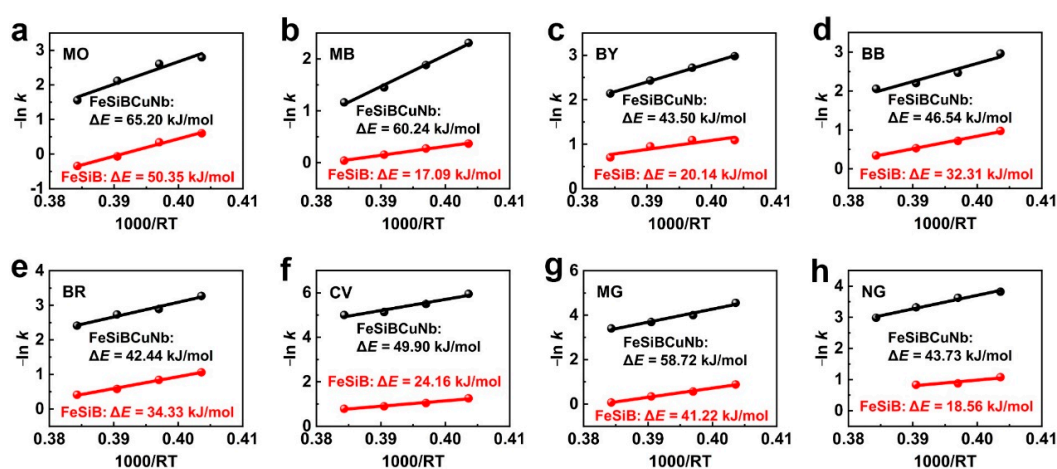


Figure 4. Activation energy ΔE of $\text{Fe}_7\text{Si}_9\text{B}_{13}$ (FeSiB) and $\text{Fe}_{73.5}\text{Si}_{13.5}\text{B}_9\text{Cu}_1\text{Nb}_3$ (FeSiBCuNb) metallic glass ribbons for (a) MO, (b) MB, (c) BY, (d) BB, (e) BR, (f) CV, (g) MG and (h) NG dyes.

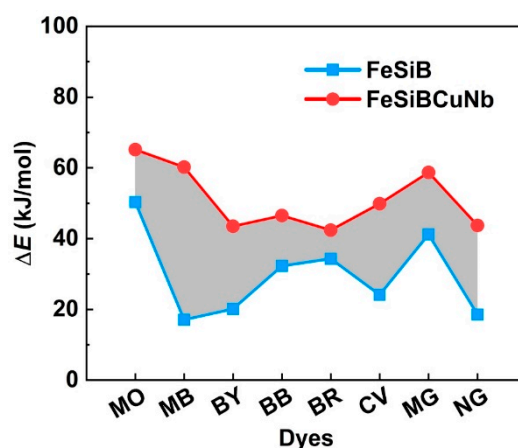


Figure 5. A summary of the activation energy ΔE values of $\text{Fe}_7\text{Si}_9\text{B}_{13}$ (FeSiB) and $\text{Fe}_{73.5}\text{Si}_{13.5}\text{B}_9\text{Cu}_1\text{Nb}_3$ (FeSiBCuNb) metallic glass ribbons for MO, MB, BY, BB, BR, CV, MG and NG dyes. Arrhenius curve fitting is based on reaction temperatures ranging from 25–40 °C.

2.3. Correlation between Metallic Glasses and H_2O_2 in Different pH

Generally, reaction parameters such as catalyst dosage, pH, dye concentration, and H_2O_2 concentration dominate the reaction efficiency in Fenton-like processes and an effective degradation of a dye solution usually involves the investigation of optimized parameters. For catalyst (metallic

glass ribbons) dosage, most of studies have demonstrated that a higher dosage of catalyst generally contributes to a higher catalytic efficiency in AOPs [24,37,53,54]. Due to the heterogeneous catalyst nature, the use of excess metallic glass ribbons only results in supplementary additional surface active sites and the release of Fe^{2+} from the ribbon surface by corrosion can be effectively controlled, which is different from the use of homogeneous Fe^{2+} as catalyst leading to a scavenging effect on the produced radicals [41]. As for dye concentration, from empirical rules, the higher concentration usually results in an inhibitory effect on the catalytic activity owing to a large amount of dye molecules covering the catalyst surface [24]. As a result, the contact between catalyst and peroxide tends to become weaker. Given the fact that most of studies only focus on a limited range of the reaction parameters (e.g., 1 mM to 10 mM H_2O_2), recently it was found that H_2O_2 concentration seems to be available in a wide allowable range (e.g., a few moles) [33]. As such, this may raise a question that what would be the practical effect regarding a much wider range of H_2O_2 concentrations?

In this work, MO was selected for the investigation of the H_2O_2 effect by $\text{Fe}_{78}\text{Si}_9\text{B}_{13}$ and $\text{Fe}_{73.5}\text{Si}_{13.5}\text{B}_9\text{Cu}_1\text{Nb}_3$ metallic glass ribbons (Figure 6). As shown in Figure 6a, $\text{Fe}_{78}\text{Si}_9\text{B}_{13}$ and a wide range of H_2O_2 concentrations from 1 mM to 0.5 M have been applied as the main Fenton reagents. When the H_2O_2 concentration increases from 1 mM to 5 mM, an apparent increase of catalytic efficiency results in full decolorization within 5 min. Consistent with many previous reports however, a further increase of H_2O_2 concentration (>5 mM) has an inhibitory effect on the catalytic efficiency due to scavenging effect of H_2O_2 on the $\bullet\text{OH}$ radicals produced, which leads to a declined catalytic activity [31]. Within the range of 1 mM to 50 mM, the decolorization of MO still reaches almost completion within 10 min. The decay of catalytic efficiency has been further enhanced using a H_2O_2 concentration of 0.5 M but the decolorization can reach more than 80% in 20 min. In comparison, the variation of H_2O_2 shows a stronger inhibitory effect on the catalytic efficiency using $\text{Fe}_{73.5}\text{Si}_{13.5}\text{B}_9\text{Cu}_1\text{Nb}_3$ as a catalyst and the range of feasible concentrations is very limited (Figure 6b). Only 1 and 2 mM H_2O_2 present optimized efficiency for the full MO decolorization in 45 min. From 5 mM to 20 mM, the inhibitory effect of H_2O_2 on decolorization is apparent. Further increasing the H_2O_2 concentration from 50 mM to 0.5 M results in negligible MO decolorization within 45 min. In both ribbons, a high H_2O_2 concentration has a detrimental effect on catalytic efficiency.

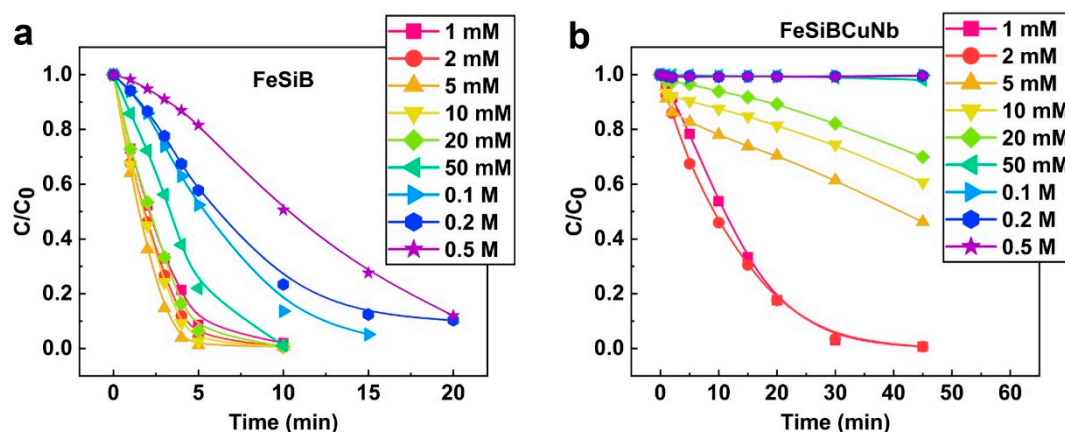


Figure 6. Effect of H_2O_2 concentrations from 1 mM to 0.5 M using (a) $\text{Fe}_{78}\text{Si}_9\text{B}_{13}$ (FeSiB) and (b) $\text{Fe}_{73.5}\text{Si}_{13.5}\text{B}_9\text{Cu}_1\text{Nb}_3$ (FeSiBCuNb) metallic glass ribbons at acidic condition (MO dye concentration: 20 ppm, catalyst dosage: 0.5 g/L, pH 3.0, 25 °C). Decolorization rates were measured from the λ_{max} of the corresponding UV-Vis spectra with reaction time.

The aforementioned results also indicate that the effect of H_2O_2 concentration depends on the type of catalysts and a catalyst with low catalytic ability (i.e., $\text{Fe}_{73.5}\text{Si}_{13.5}\text{B}_9\text{Cu}_1\text{Nb}_3$) is more sensitive to the variation of H_2O_2 concentration. Figure 7 has shown the corresponding reaction rate constant (k) of $\text{Fe}_{78}\text{Si}_9\text{B}_{13}$ and $\text{Fe}_{73.5}\text{Si}_{13.5}\text{B}_9\text{Cu}_1\text{Nb}_3$ metallic glass ribbons as a function of initial H_2O_2

concentration ($[H_2O_2]_0$). The k of $Fe_{78}Si_9B_{13}$ are almost one order of magnitude higher than that of $Fe_{73.5}Si_{13.5}B_9Cu_1Nb_3$, and $Fe_{78}Si_9B_{13}$ can perform a better catalytic efficiency at a wider range of H_2O_2 concentration. However, both of them have an inhibitory catalytic effect at a H_2O_2 concentration higher than 5 mM.

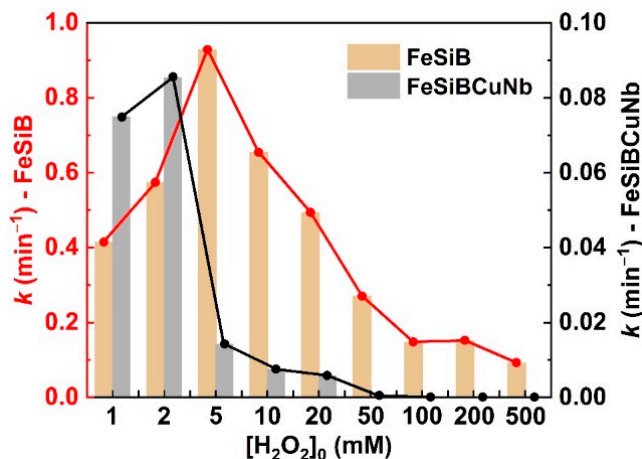


Figure 7. Reaction rate constants (k) of $Fe_{78}Si_9B_{13}$ (FeSiB) and $Fe_{73.5}Si_{13.5}B_9Cu_1Nb_3$ (FeSiBCuNb) metallic glass ribbons as a function of initial H_2O_2 concentration ($[H_2O_2]_0$) ranging from 1 mM to 500 mM (or 0.5 M) in the degradation of MO dye (dye concentration: 20 ppm, catalyst dosage: 0.5 g/L, pH 3.0, 25 °C).

It should be noticed that Fenton-like processes usually rely on acidic conditions to maintain a reliable catalytic performance. pH 3.0 is typically used for most iron-containing catalysts, including the Fe-based metallic glasses used in this work. Under weaker acidic conditions (e.g., pH 4.0), the catalytic efficiency will decline and it will be further inhibited under neutral conditions. Figure 8a,b show the catalytic performance of the two metallic glass ribbons used under neutral conditions (pH 6.2 ± 0.1) with different H_2O_2 concentrations. Both of them exhibit unapparent decolorization of MO dye, indicating that the neutral condition is unfavorable for Fenton-like processes using metallic glass ribbons [24]. At a high concentration of H_2O_2 (0.5 M), the catalytic efficiency is also very low, with 15% and 0% of decolorization rate for $Fe_{78}Si_9B_{13}$ and $Fe_{73.5}Si_{13.5}B_9Cu_1Nb_3$, respectively, after 60 min (Figure 8c). However, it has been reported that Fenton-like processes with UV-Vis irradiation can highly enhance their color removal rates under neutral conditions [33]. Accordingly, Figure 9a,b suggest that a low concentration of H_2O_2 (50 mM) with UV-Vis irradiation does not effectively promote the decolorization rate but the combination of high H_2O_2 concentration and UV-Vis irradiation effectively enhances the decolorization rate. At 1.0 M H_2O_2 , both metallic glass ribbons do not exhibit a big difference in MO decolorization, which reaches up to 94% and 90% for $Fe_{78}Si_9B_{13}$ and $Fe_{73.5}Si_{13.5}B_9Cu_1Nb_3$, respectively, within 60 min. Increasing the H_2O_2 concentration under UV-Vis irradiation leading to promoted dye degradation rate reveals that the combination of high concentration of H_2O_2 and irradiation can overcome the catalytic efficiency limitation under neutral conditions.

Further investigation indicates that in addition to a photo-enhancement effect, the improved efficiency is also attributable to the effective optimization of pH conditions with increasing H_2O_2 concentration (Figure 9c,d). Accordingly, this behavior provides a novel strategy to overcome the limitation of Fenton-like processes under neutral conditions.

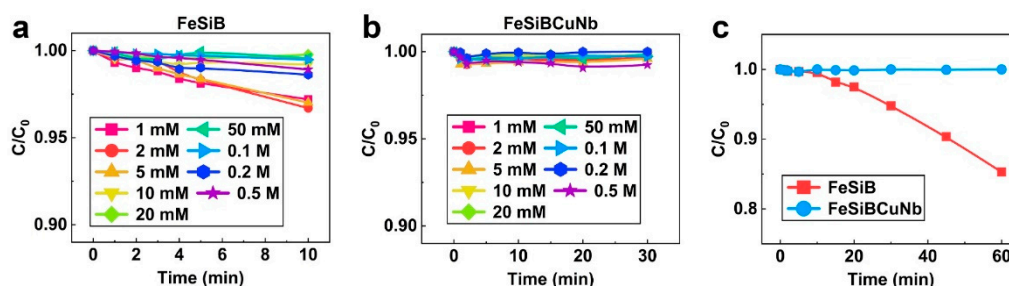


Figure 8. Effect of H_2O_2 concentration from 1 mM to 0.5 M using (a) $Fe_{78}Si_9B_{13}$ (FeSiB) and (b) $Fe_{73.5}Si_{13.5}B_9Cu_1Nb_3$ (FeSiBCuNb) metallic glass ribbons under neutral conditions. (c) Comparison of MO degradation by $Fe_{78}Si_9B_{13}$ (FeSiB) and $Fe_{73.5}Si_{13.5}B_9Cu_1Nb_3$ (FeSiBCuNb) at 0.5 M H_2O_2 and neutral condition (MO dye concentration: 20 ppm, catalyst dosage: 0.5 g/L, pH 6.2 (± 0.1), 25 °C). Decolorization rates were measured from the λ_{max} of the corresponding UV-Vis spectra with reaction time.

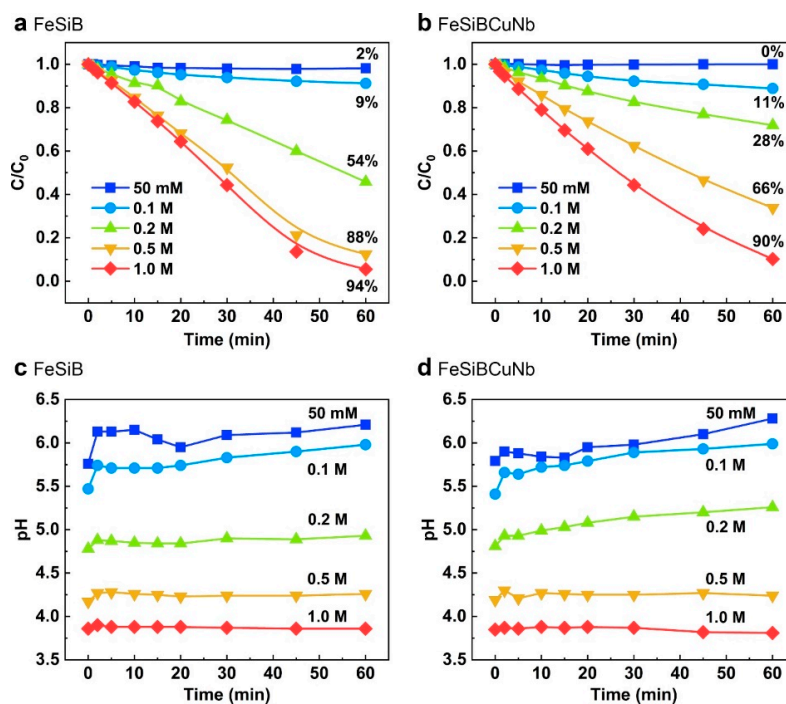


Figure 9. Effect of H_2O_2 concentrations by (a) $Fe_{78}Si_9B_{13}$ (FeSiB) and (b) $Fe_{73.5}Si_{13.5}B_9Cu_1Nb_3$ (FeSiBCuNb) metallic glass ribbons (0.5 g/L) under neutral conditions (pH 6.2 \pm 0.1) and UV-Vis irradiation ($7.7 \mu W/cm^2$). (c,d) pH variation along reaction time corresponding to (a,b), respectively. Decolorization rates were measured from the λ_{max} of the corresponding UV-Vis spectra with reaction time.

2.4. Correlation between Decolorization and Mineralization

Figure 10a–h show the decolorization processes of the eight dyes using $Fe_{78}Si_9B_{13}$ metallic glass ribbons during 5 min. The full wavelength UV-Vis spectra (190–800 nm) clearly indicate that most of dyes have experienced an effective destruction of their chromophore groups by the $Fe_{78}Si_9B_{13}$ -activated Fenton-like process [42]. It should be noted that the initial absorbance peak of NG is located at 714 nm but it has shifted to 408 nm after the Fenton-like process is activated, which is also reported by sulfate radical-based AOPs [50]. After 5 min, the intensities of the characteristic absorbance peaks of the dyes become weaker and then disappear, except for CV and MG dyes. Both CV and MG dyes have

a slower decolorization efficiency than the other dyes, which becomes more apparent when using $\text{Fe}_{73.5}\text{Si}_{13.5}\text{B}_9\text{Cu}_1\text{Nb}_3$ metallic glass. Figure 10i–p also show the decolorization processes of the eight dyes using $\text{Fe}_{73.5}\text{Si}_{13.5}\text{B}_9\text{Cu}_1\text{Nb}_3$ metallic glass. The decolorization efficiencies are slower and the peaks disappear after 30 min. The decay of the characteristic absorbance peaks is even slower regarding CV and MG dyes (Figure 10n,o). Considering the dye structure, it can be concluded that triarylmethane dyes are unfavorable in the Fenton-like system with Fe-based metallic glass ribbons.

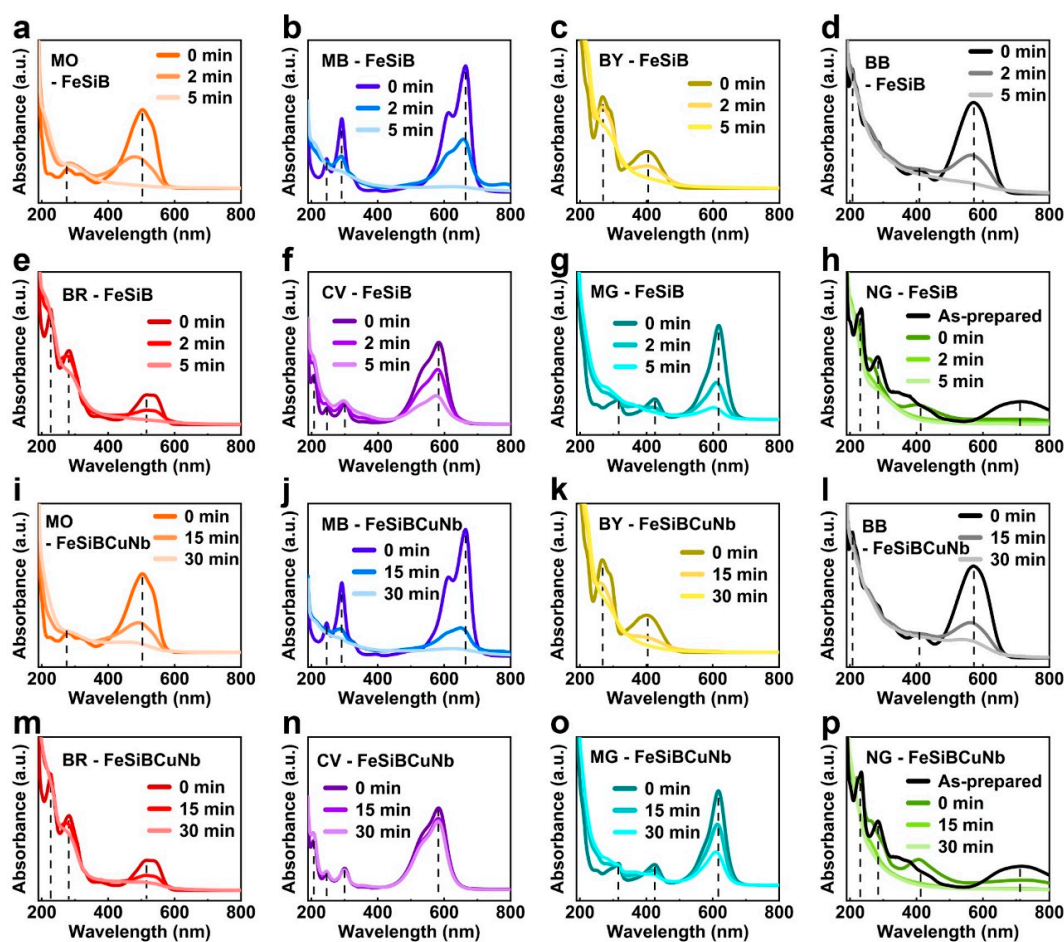


Figure 10. UV-Vis spectra of (a) MO, (b) MB, (c) BY, (d) BB, (e) BR (f) CV, (g) MG and (h) NG dye degradation by $\text{Fe}_{78}\text{Si}_9\text{B}_{13}$ (FeSiB) within 5 min. UV-Vis spectra of (i) MO, (j) MB, (k) BY, (l) BB, (m) BR (n) CV, (o) MG and (p) NG dye degradation by $\text{Fe}_{73.5}\text{Si}_{13.5}\text{B}_9\text{Cu}_1\text{Nb}_3$ (FeSiBCuNb) within 30 min. (dye concentration: 20 ppm, catalyst dosage: 0.5 g/L, H_2O_2 concentration: 1 mM, pH 3.0).

Although the decolorization efficiencies of dyes in the Vis spectra provide an important clue about the catalytic ability by catalysts or the catalytic efficiency of the reaction system, they only include the destruction of chromophore group in dye molecules. To fully convert organic pollutants into harmless substances (CO_2 , H_2O , etc.), the degradation pathway is much more complicated. In Figure 10, it can be seen that the absorbance peaks at UV region also become inapparent along with peaks at the Vis region. The disappearance of UV peaks reveals that the Fenton-like process not only effectively destroys the chromophore groups in the dye structures, but only involves catalytic oxidation of the aromatic structure [55]. This behavior can be further confirmed by the TOC removal rate ($[\text{TOC}]/[\text{TOC}]_0$), which is usually employed to evaluate the mineralization rate in AOPs [16,42].

Figure 11 shows that most of dye mineralization rates reach about 40% within 15 min when using $\text{Fe}_{78}\text{Si}_9\text{B}_{13}$ metallic glass ribbons while for $\text{Fe}_{73.5}\text{Si}_{13.5}\text{B}_9\text{Cu}_1\text{Nb}_3$ metallic glass ribbons, a much lower TOC removal rate can be seen. Both $\text{Fe}_{78}\text{Si}_9\text{B}_{13}$ and $\text{Fe}_{73.5}\text{Si}_{13.5}\text{B}_9\text{Cu}_1\text{Nb}_3$ have a relatively higher TOC

removal rate for MO and have a relatively lower TOC removal rate for MG. The lowest TOC removal rate occurs for CV and MG dyes using $\text{Fe}_{73.5}\text{Si}_{13.5}\text{B}_9\text{Cu}_1\text{Nb}_3$. According to the TOC removal rates of the eight dyes, the average values of $\text{Fe}_{78}\text{Si}_9\text{B}_{13}$ and $\text{Fe}_{73.5}\text{Si}_{13.5}\text{B}_9\text{Cu}_1\text{Nb}_3$ metallic glasses are calculated as 42.7% and 12.6%, respectively, indicating most of dye degradations can achieve TOC removal rates close to average value using specific metallic glass ribbons. In addition, the mineralization rate is apparently closely related to decolorization, where most of time, a fast decolorization usually leads to a higher mineralization rate, corresponding to the decolorization efficiency shown in Figures 2 and 3.

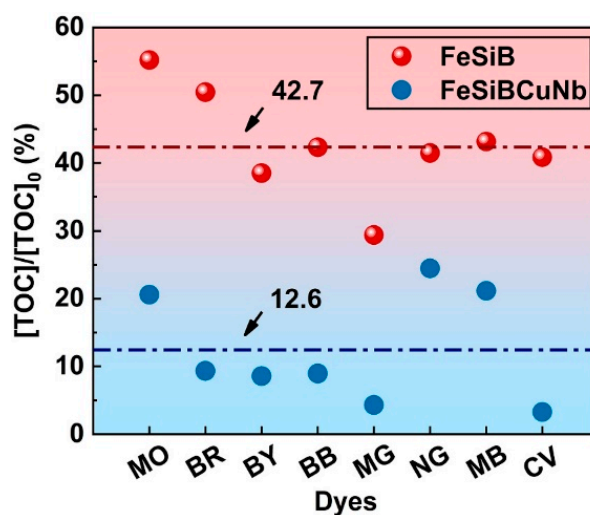


Figure 11. TOC removal rate ($[\text{TOC}]/[\text{TOC}]_0$) of eight dyes using $\text{Fe}_{78}\text{Si}_9\text{B}_{13}$ (FeSiB) and $\text{Fe}_{73.5}\text{Si}_{13.5}\text{B}_9\text{Cu}_1\text{Nb}_3$ (FeSiBCuNb) after 15 min.

The dominant reactive species in Fe-based metallic glasses-activated Fenton-like processes have been reported to be $\bullet\text{OH}$ [33,56–58]. The effective decolorization and mineralization in this work suggest that part of the dye molecules involved with $\bullet\text{OH}$ have experienced degradation pathways including cleavage of chromophore groups, formation of intermediates, further oxidation of intermediates to become CO_2 , H_2O and inorganic substances [59]. For example, the main degradation mechanism of MG dye (a triarylmethane dye) in the Fenton-like process probably involves the cleavage of the conjugated chromophore structure by attack of $\bullet\text{OH}$, followed by N-demethylation reactions and opening of phenyl rings to become smaller molecules [49,60], although different reaction routes may still vary according to the specific reaction conditions; the main degradation mechanism of MO dye (an azo dye) goes through the initial destruction of the azo chromophore group ($-\text{N}=\text{N}-$) to form smaller intermediates with functional amine ($-\text{N}(\text{CH}_3)_2$) and sulfonate ($-\text{SO}_3^-$) groups leading to fast decolorization, followed by the demethylation of intermediates, the hydroxylation of aromatic rings, and further ring opening [61,62]. Given the fact that a low dosage of metallic glass ribbons is used in this work, their structure and surface may have a minor direct effect on dye degradation but their catalytic activation toward H_2O_2 directly affects the decolorization and further mineralization rate of dyes due to the production rate of $\bullet\text{OH}$ when using different metallic glass ribbons [16,22]. The intrinsic catalytic activity of the metallic glass dominates the dye degradation efficiency in this work.

3. Materials and Methods

3.1. Materials and Chemicals

Metallic glass ribbons with nominal chemical compositions of $\text{Fe}_{78}\text{Si}_9\text{B}_{13}$ and $\text{Fe}_{73.5}\text{Si}_{13.5}\text{B}_9\text{Cu}_1\text{Nb}_3$ were supplied by Qingdao Yunlu Energy Technology Co., Ltd. (Qingdao, China), and were manufactured by the melt spinning technique. For the preparation procedures of as-spun metallic glass ribbons readers may refer to a previous report [53]. The produced ribbons generally have a

thickness of 30–40 μm and were cut into pieces of 10×20 mm (width and length), respectively, for the following catalytic analysis with dyes. BB, BY and BR, hydrochloric acid (HCl, 37% *w/w*) were purchased from Sigma-Aldrich (Sydney, Australia). MO and MB were supplied by Xilong Chemical Co., Ltd. (Shantou, China). CV and NG were supplied by Wenzhou Huaqiao Chemical Reagent Co., Ltd. (Wenzhou, China). MG was purchased from Ji'an Haomai Fine Chemical Industry Co., Ltd. (Ji'an, China). Hydrogen peroxide (H_2O_2 , 30 wt%) and sodium hydroxide (NaOH, 40% *w/v*) were purchased from Rowe Scientific Pty Ltd. (Perth, Australia). Milli-Q water with $18.2 \text{ M}\Omega\cdot\text{cm}$ was used for catalytic processes, dilution and cleaning.

3.2. Characterization

The internal structure of as-spun $\text{Fe}_{78}\text{Si}_9\text{B}_{13}$ and $\text{Fe}_{73.5}\text{Si}_{13.5}\text{B}_9\text{Cu}_1\text{Nb}_3$ metallic glass ribbons have been well characterized by X-ray diffraction (XRD), differential scanning calorimetry (DSC) and transmission electron microscopy (TEM) in our previous work [53], which demonstrated their fully amorphous nature.

3.3. Catalytic Analysis

The catalytic oxidation of dyes by Fenton-like processes was investigated with involvement of two as-spun Fe-based metallic glass ribbons and different concentrations of H_2O_2 in a thermostatic water bath. The catalytic thermal behavior of Fe-based metallic glass ribbons therefore could be studied under controlled temperatures (i.e., 25, 30, 35, 40 $^\circ\text{C}$). Before each experiment, 20 ppm dye solution was freshly prepared by submitting 2 mL of pre-prepared 1000 ppm dye to dilution to 100 mL. The stirring rate was fixed at 300 rpm throughout this work. Except for the initial pH 6.2 (± 0.1) of as-prepared MO dye solution, all other pH values were controlled at 3.0 as initial pH by adding diluted HCl solution. The pH values in Figure 9c,d were measured after addition of specific concentration of H_2O_2 without Fe-based metallic glasses and irradiation. The measurement was obtained by monitoring of a pH meter after extracting a specific volume of solution at that time. The effect of H_2O_2 concentration on the Fenton-like process was analyzed over a wide range (1 mM–1 M) of UV-Vis irradiation using a 300 W xenon simulated solar light lamp (Perfectlight Scientific Pty Ltd., Beijing, China) applied to enhance the catalytic behavior of the Fe-based metallic glass ribbons. According to the specific absorbance peak (λ_{max}) of dyes in the visible spectrum, the decolorization of dyes could be quantified by UV-Vis spectrometry (Lambda 35, Perkin Elmer, Shelton, CT, USA), where each sample (3.5 mL) was extracted from reacting solution and characterized immediately at predetermined time intervals. Total organic carbon (TOC) removal rates before and after the Fenton-like process were measured by a TOC analyzer (TOC-L_{CPH}, Shimadzu, Sydney, Australia).

4. Conclusions

In summary, a wide range of dyes including azo dyes (i.e., MO, BB, BY and BR), a thiazine dye (i.e., MB), triarylmethane dyes (i.e., MG and CV) and a nitroso dye (i.e., NG) have been selected to investigate their degradation by two Fe-based ($\text{Fe}_{78}\text{Si}_9\text{B}_{13}$ and $\text{Fe}_{73.5}\text{Si}_{13.5}\text{B}_9\text{Cu}_1\text{Nb}_3$) metallic glasses activated Fenton-like processes, which aims to get a systematic understanding of the correlation of the metallic glasses with dye degradation, focusing on the thermal catalytic behavior, H_2O_2 concentration at different pH values, decolorization and mineralization. The following points shed light on the significance in this work:

- The correlation of the thermal catalytic behavior between metallic glasses and dyes has been revealed, where $\text{Fe}_{78}\text{Si}_9\text{B}_{13}$ metallic glass ribbons with active catalytic ability have a lower activation energy (ΔE) than that of $\text{Fe}_{73.5}\text{Si}_{13.5}\text{B}_9\text{Cu}_1\text{Nb}_3$ in all dye degradations, and the ΔE of the metallic glass depends on the reaction environment (dyes).
- Under acidic conditions, a high H_2O_2 concentration is unfavorable to catalytic activity. However, under neutral conditions, a photo-enhanced Fenton-like process catalyzed by Fe-based metallic

glasses facilitates dye degradation at higher concentrations of H₂O₂ due to the decrease of pH and enhancement of irradiation.

- Fe₇₈Si₉B₁₃ metallic glass ribbons achieve an average TOC removal rate of 42.7% dye degradation in 15 min, which is higher than Fe_{73.5}Si_{13.5}B₉Cu₁Nb₃ (12.6%). The decolorization rate is closely related to the mineralization rate.

Author Contributions: Conceptualization, X.W., S.-X.L. and L.-C.Z.; Formal analysis, X.W., Q.Z., S.-X.L., Z.J., W.Z., W.W. and L.-C.Z.; Funding acquisition, W.W. and L.-C.Z.; Methodology, X.W., S.-X.L. and L.-C.Z.; Writing—original draft, X.W., S.-X.L. and L.-C.Z.; Writing—review and editing, X.W., Q.Z., S.-X.L., Z.J., W.Z., W.W. and L.-C.Z. All authors have read and agreed to the published version of the manuscript.

Funding: Financial supports from Australian Research Council Discovery Project [DP130103592] and National Natural Science Foundation of China (Grant Nos. 61671206, 51771103) are gratefully acknowledged.

Conflicts of Interest: The authors declare no conflict of interest.

References

1. Zhang, L.C.; Jia, Z.; Lyu, F.; Liang, S.X.; Lu, J. A review of catalytic performance of metallic glasses in wastewater treatment: Recent progress and prospects. *Prog. Mater. Sci.* **2019**, *105*, 100576. [[CrossRef](#)]
2. Qiao, J.C.; Wang, Q.; Pelletier, J.M.; Kato, H.; Casalini, R.; Crespo, D.; Pineda, E.; Yao, Y.; Yang, Y. Structural heterogeneities and mechanical behavior of amorphous alloys. *Prog. Mater. Sci.* **2019**, *104*, 250–329. [[CrossRef](#)]
3. Wang, J.Q.; Liu, Y.H.; Chen, M.W.; Louzguine-Luzgin, D.V.; Inoue, A.; Perepezko, J.H. Excellent capability in degrading azo dyes by MgZn-Based metallic glass powders. *Sci. Rep.* **2012**, *2*, 418. [[CrossRef](#)] [[PubMed](#)]
4. Qiao, J.C.; Wang, Y.J.; Pelletier, J.M.; Keer, L.M.; Fine, M.E.; Yao, Y. Characteristics of stress relaxation kinetics of La₆₀Ni₁₅Al₂₅ bulk metallic glass. *Acta Mater.* **2015**, *98*, 43–50. [[CrossRef](#)]
5. Hu, F.; Zhu, S.; Chen, S.; Li, Y.; Ma, L.; Wu, T.; Zhang, Y.; Wang, C.; Liu, C.; Yang, X.; et al. Amorphous metallic NiFeP: A conductive bulk material achieving high activity for oxygen evolution reaction in both alkaline and acidic media. *Adv. Mater.* **2017**, *29*, 1606570. [[CrossRef](#)]
6. Jia, Z.; Duan, X.; Qin, P.; Zhang, W.; Wang, W.; Yang, C.; Sun, H.; Wang, S.; Zhang, L.C. Disordered atomic packing structure of metallic glass: Toward ultrafast hydroxyl radicals production rate and strong electron transfer ability in catalytic performance. *Adv. Funct. Mater.* **2017**, *27*, 1702258. [[CrossRef](#)]
7. Wang, J.Q.; Liu, Y.H.; Chen, M.W.; Xie, G.Q.; Louzguine-Luzgin, D.V.; Inoue, A.; Perepezko, J.H. Rapid degradation of azo dye by Fe-based metallic glass powder. *Adv. Funct. Mater.* **2012**, *22*, 2567–2570. [[CrossRef](#)]
8. Hu, Y.C.; Wang, Y.Z.; Su, R.; Cao, C.R.; Li, F.; Sun, C.W.; Yang, Y.; Guan, P.F.; Ding, D.W.; Wang, Z.L.; et al. A highly efficient and self-stabilizing metallic-glass catalyst for electrochemical hydrogen generation. *Adv. Mater.* **2016**, *28*, 10293–10297. [[CrossRef](#)]
9. Jia, Z.; Wang, Q.; Sun, L.; Wang, Q.; Zhang, L.C.; Wu, G.; Luan, J.H.; Jiao, Z.B.; Wang, A.; Liang, S.X.; et al. Attractive in situ self-reconstructed hierarchical gradient structure of metallic glass for high efficiency and remarkable stability in catalytic performance. *Adv. Funct. Mater.* **2019**, *29*, 1807857. [[CrossRef](#)]
10. Miao, F.; Wang, Q.Q.; Zeng, Q.S.; Hou, L.; Liang, T.; Cui, Z.Q.; Shen, B.L. Excellent reusability of FeBC amorphous ribbons induced by progressive formation of through-pore structure during acid orange 7 degradation. *J. Mater. Sci. Technol.* **2020**, *38*, 107–118. [[CrossRef](#)]
11. Lu, S.; Lian, J.; Zhang, F.; Jiang, W.; Hu, Q.; Li, D.; Zhang, B. Fe₄₀Co₄₀Se₂₀ glassy films supported on carbon fiber paper as electrocatalysts in the oxygen evolution reaction. *J. Electrochem. Soc.* **2019**, *166*, F620–F626. [[CrossRef](#)]
12. Tan, Y.; Zhu, F.; Wang, H.; Tian, Y.; Hirata, A.; Fujita, T.; Chen, M. Noble-metal-free metallic glass as a highly active and stable bifunctional electrocatalyst for water splitting. *Adv. Mater. Interfaces* **2017**, *4*, 1601086. [[CrossRef](#)]
13. Zhang, F.; Wu, J.; Jiang, W.; Hu, Q.; Zhang, B. New and efficient electrocatalyst for hydrogen production from water splitting: Inexpensive, robust metallic glassy ribbons based on iron and cobalt. *ACS Appl. Mater. Interfaces* **2017**, *9*, 31340–31344. [[CrossRef](#)] [[PubMed](#)]
14. Lv, C.; Yan, C.; Chen, G.; Ding, Y.; Sun, J.; Zhou, Y.; Yu, G. An amorphous noble-metal-free electrocatalyst that enables nitrogen fixation under ambient conditions. *Angew. Chem. Int. Ed.* **2018**, *57*, 6073–6076. [[CrossRef](#)]

15. Zhang, L.C.; Liang, S.X. Fe-based metallic glasses in functional catalytic applications. *Chem. Asian J.* **2018**, *13*, 3575–3592. [[CrossRef](#)]
16. Liang, S.X.; Jia, Z.; Zhang, W.C.; Li, X.F.; Wang, W.M.; Lin, H.C.; Zhang, L.C. Ultrafast activation efficiency of three peroxides by Fe₇₈Si₉B₁₃ metallic glass under photo-enhanced catalytic oxidation: A comparative study. *Appl. Catal. B* **2018**, *221*, 108–118. [[CrossRef](#)]
17. Saratale, R.G.; Saratale, G.D.; Chang, J.S.; Govindwar, S.P. Bacterial decolorization and degradation of azo dyes: A review. *J. Taiwan Inst. Chem. Eng.* **2011**, *42*, 138–157. [[CrossRef](#)]
18. Silva, G.C.; Ciminelli, V.S.T.; Ferreira, A.M.; Pissolati, N.C.; Paiva, P.R.P.; López, J.L. A facile synthesis of Mn₃O₄/Fe₃O₄ superparamagnetic nanocomposites by chemical precipitation: Characterization and application in dye degradation. *Mater. Res. Bull.* **2014**, *49*, 544–551. [[CrossRef](#)]
19. Karcher, S.; Kornmüller, A.; Jekel, M. Anion exchange resins for removal of reactive dyes from textile wastewaters. *Water Res.* **2002**, *36*, 4717–4724. [[CrossRef](#)]
20. Chen, L.Y.; Xu, T.; Lu, S.; Wang, Z.X.; Chen, S.; Zhang, L. Improved hardness and wear resistance of plasma sprayed nanostructured NiCrBSi coating via short-time heat treatment. *Surf. Coat. Technol.* **2018**, *350*, 436–444. [[CrossRef](#)]
21. Lindsey, M.E.; Tarr, M.A. Quantitation of hydroxyl radical during Fenton oxidation following a single addition of iron and peroxide. *Chemosphere* **2000**, *41*, 409–417. [[CrossRef](#)]
22. Jia, Z.; Kang, J.; Zhang, W.C.; Wang, W.M.; Yang, C.; Sun, H.; Habibi, D.; Zhang, L.C. Surface aging behaviour of Fe-based amorphous alloys as catalysts during heterogeneous photo Fenton-like process for water treatment. *Appl. Catal. B* **2017**, *204*, 537–547. [[CrossRef](#)]
23. Liang, S.X.; Zhang, W.; Wang, W.; Jia, G.; Yang, W.; Zhang, L.C. Surface reactivation of FeNiPC metallic glass: A strategy for highly enhanced catalytic behavior. *J. Phys. Chem. Solids* **2019**, *132*, 89–98. [[CrossRef](#)]
24. Wang, Q.Q.; Chen, M.X.; Lin, P.H.; Cui, Z.Q.; Chu, C.L.; Shen, B.L. Investigation of FePC amorphous alloys with self-renewing behaviour for highly efficient decolorization of methylene blue. *J. Mater. Chem. A* **2018**, *6*, 10686–10699. [[CrossRef](#)]
25. Wang, Q.Q.; Chen, M.X.; Shao, L.L.; Ge, Y.W.; Lin, P.H.; Chu, C.L.; Shen, B.L. Effects of structural relaxation on the dye degradation ability of FePC amorphous alloys. *J. Non-Cryst. Solids* **2019**, *525*, 119671. [[CrossRef](#)]
26. Liang, S.X.; Zhang, W.; Zhang, L.; Wang, W.; Zhang, L.C. Remediation of industrial contaminated water with arsenic and nitrate by mass-produced Fe-based metallic glass: Toward potential industrial applications. *Sustain. Mater. Technol.* **2019**, *22*, e00126. [[CrossRef](#)]
27. Ju, Y.; Yang, S.; Ding, Y.; Sun, C.; Zhang, A.; Wang, L. Microwave-assisted rapid photocatalytic degradation of malachite green in TiO₂ suspensions: Mechanism and pathways. *J. Phys. Chem. A* **2008**, *112*, 11172–11177. [[CrossRef](#)]
28. Nidheesh, P.V.; Gandhimathi, R.; Ramesh, S.T. Degradation of dyes from aqueous solution by Fenton processes: A review. *Environ. Sci. Pollut. Res.* **2013**, *20*, 2099–2132. [[CrossRef](#)]
29. Moussavi, G.; Mahmoudi, M. Removal of azo and anthraquinone reactive dyes from industrial wastewaters using MgO nanoparticles. *J. Hazard. Mater.* **2009**, *168*, 806–812. [[CrossRef](#)]
30. Oliveira, E.; Bértolo, E.; Núñez, C.; Pilla, V.; Santos, H.M.; Fernández-Lodeiro, J.; Fernández-Lodeiro, A.; Djafari, J.; Capelo, J.L.; Lodeiro, C. Green and red fluorescent dyes for translational applications in imaging and sensing analytes: A dual-color flag. *ChemistryOpen* **2018**, *7*, 9–52. [[CrossRef](#)]
31. Ramirez, J.H.; Maldonado-Hódar, F.J.; Pérez-Cadenas, A.F.; Moreno-Castilla, C.; Costa, C.A.; Madeira, L.M. Azo-dye orange II degradation by heterogeneous Fenton-like reaction using carbon-Fe catalysts. *Appl. Catal. B* **2007**, *75*, 312–323. [[CrossRef](#)]
32. Bafana, A.; Saravana Devi, S.; Chakrabarti, T. Azo dyes: Past, present and the future. *Environ. Rev.* **2011**, *19*, 350–370. [[CrossRef](#)]
33. Jia, Z.; Zhang, W.C.; Wang, W.M.; Habibi, D.; Zhang, L.C. Amorphous Fe₇₈Si₉B₁₃ alloy: An efficient and reusable photo-enhanced Fenton-like catalyst in degradation of cibacron brilliant red 3B-A dye under UV–vis light. *Appl. Catal. B* **2016**, *192*, 46–56. [[CrossRef](#)]
34. Yang, C.; Zhang, C.; Liu, L. Excellent degradation performance of 3D hierarchical nanoporous structures of copper towards organic pollutants. *J. Mater. Chem. A* **2018**, *6*, 20992–21002. [[CrossRef](#)]
35. Paciullo, C.A.; Horner, D.M.; Hatton, K.W.; Flynn, J.D. Methylene blue for the treatment of septic shock. *Pharmacotherapy* **2010**, *30*, 702–715. [[CrossRef](#)] [[PubMed](#)]

36. Jia, Z.; Lyu, F.; Zhang, L.C.; Zeng, S.; Liang, S.X.; Li, Y.Y.; Lu, J. Pt nanoparticles decorated heterostructured g-C₃N₄/Bi₂MoO₆ microplates with highly enhanced photocatalytic activities under visible light. *Sci. Rep.* **2019**, *9*, 7636. [[CrossRef](#)] [[PubMed](#)]
37. Hou, L.; Wang, Q.Q.; Fan, X.D.; Miao, F.; Yang, W.M.; Shen, B.L. Effect of Co addition on catalytic activity of FePCCu amorphous alloy for methylene blue degradation. *New J. Chem.* **2019**, *43*, 6126–6135. [[CrossRef](#)]
38. Yang, W.M.; Wang, Q.Q.; Li, W.Y.; Xue, L.; Liu, H.S.; Zhou, J.; Mo, J.Y.; Shen, B.L. A novel thermal-tuning Fe-based amorphous alloy for automatically recycled methylene blue degradation. *Mater. Des.* **2019**, *161*, 136–146. [[CrossRef](#)]
39. Chen, C.C.; Chen, W.C.; Chiou, M.R.; Chen, S.W.; Chen, Y.Y.; Fan, H.J. Degradation of crystal violet by an FeGAC/H₂O₂ process. *J. Hazard. Mater.* **2011**, *196*, 420–425. [[CrossRef](#)]
40. Liang, S.X.; Jia, Z.; Zhang, W.C.; Wang, W.M.; Zhang, L.C. Rapid malachite green degradation using Fe_{73.5}Si_{13.5}B₉Cu₁Nb₃ metallic glass for activation of persulfate under UV-vis light. *Mater. Des.* **2017**, *119*, 244–253. [[CrossRef](#)]
41. Kusic, H.; Peternel, I.; Ukc, S.; Koprivanac, N.; Bolanca, T.; Papic, S.; Bozic, A.L. Modeling of iron activated persulfate oxidation treating reactive azo dye in water matrix. *Chem. Eng. J.* **2011**, *172*, 109–121. [[CrossRef](#)]
42. Bae, S.; Kim, S.; Lee, S.; Choi, W. Dye decolorization test for the activity assessment of visible light photocatalysts: Realities and limitations. *Catal. Today* **2014**, *224*, 21–28. [[CrossRef](#)]
43. Wang, J.C.; Liang, S.X.; Jia, Z.; Zhang, W.C.; Wang, W.M.; Liu, Y.J.; Lu, J.; Zhang, L. Chemically dealloyed Fe-based metallic glass with void channels-like architecture for highly enhanced peroxymonosulfate activation in catalysis. *J. Alloys Compd.* **2019**, *785*, 642–650. [[CrossRef](#)]
44. Jia, Z.; La, L.B.T.; Zhang, W.C.; Liang, S.X.; Jiang, B.; Xie, S.K.; Habibi, D.; Zhang, L.C. Strong enhancement on dye photocatalytic degradation by ball-milled TiO₂: A study of cationic and anionic dyes. *J. Mater. Sci. Technol.* **2017**, *33*, 856–863. [[CrossRef](#)]
45. Jia, Z.; Wang, J.C.; Liang, S.X.; Zhang, W.C.; Wang, W.M.; Zhang, L. Activation of peroxymonosulfate by Fe₇₈Si₉B₁₃ metallic glass: The influence of crystallization. *J. Alloys Compd.* **2017**, *728*, 525–533. [[CrossRef](#)]
46. Jia, Z.; Miao, J.; Lu, H.B.; Habibi, D.; Zhang, W.C.; Zhang, L.C. Photocatalytic degradation and absorption kinetics of cibacron brilliant yellow 3G-P by nanosized ZnO catalyst under simulated solar light. *J. Taiwan Inst. Chem. Eng.* **2016**, *60*, 267–274. [[CrossRef](#)]
47. Jia, Z.; Liang, S.X.; Zhang, W.C.; Wang, W.M.; Yang, C.; Zhang, L. Heterogeneous photo Fenton-like degradation of cibacron brilliant red 3b-A dye using amorphous Fe₇₈Si₉B₁₃ and Fe_{73.5}Si_{13.5}B₉Cu₁Nb₃ alloys: The influence of adsorption. *J. Taiwan Inst. Chem. Eng.* **2017**, *71*, 128–136. [[CrossRef](#)]
48. Liu, X.; Zhang, T.; Xu, D.; Zhang, L. Microwave-assisted catalytic degradation of crystal violet with barium ferrite nanomaterial. *Ind. Eng. Chem. Res.* **2016**, *55*, 11869–11877. [[CrossRef](#)]
49. Ju, Y.; Yang, S.; Ding, Y.; Sun, C.; Gu, C.; He, Z.; Qin, C.; He, H.; Xu, B. Microwave-enhanced H₂O₂-based process for treating aqueous malachite green solutions: Intermediates and degradation mechanism. *J. Hazard. Mater.* **2009**, *171*, 123–132. [[CrossRef](#)]
50. Li, X.F.; Liang, S.X.; Xi, X.W.; Jia, Z.; Xie, S.K.; Lin, H.C.; Hu, J.P.; Zhang, L. Excellent performance of Fe₇₈Si₉B₁₃ metallic glass for activating peroxymonosulfate in degradation of naphthol green B. *Metals* **2017**, *7*, 273. [[CrossRef](#)]
51. Wang, J.C.; Jia, Z.; Liang, S.X.; Qin, P.; Zhang, W.C.; Wang, W.M.; Sercombe, T.B.; Zhang, L. Fe_{73.5}Si_{13.5}B₉Cu₁Nb₃ metallic glass: Rapid activation of peroxymonosulfate towards ultrafast eosin Y degradation. *Mater. Des.* **2018**, *140*, 73–84. [[CrossRef](#)]
52. Li, R.; Liu, X.J.; Wang, H.; Wu, Y.; Chan, K.C.; Lu, Z.P. Flexible glassy grid structure for rapid degradation of azo dye. *Mater. Des.* **2018**, *155*, 346–351. [[CrossRef](#)]
53. Liang, S.X.; Jia, Z.; Liu, Y.J.; Zhang, W.; Wang, W.; Lu, J.; Zhang, L.C. Compelling rejuvenated catalytic performance in metallic glasses. *Adv. Mater.* **2018**, *30*, 1802764. [[CrossRef](#)] [[PubMed](#)]
54. Jia, Z.; Duan, X.; Zhang, W.; Wang, W.; Sun, H.; Wang, S.; Zhang, L.C. Ultra-sustainable Fe₇₈Si₉B₁₃ metallic glass as a catalyst for activation of persulfate on methylene blue degradation under UV-vis light. *Sci. Rep.* **2016**, *6*, 38520. [[CrossRef](#)]
55. Zhang, C.; Sun, Q.; Liu, K. From adsorption to reductive degradation: Different decolorization properties of metallic glasses based on different iron-group elements. *J. Alloys Compd.* **2018**, *741*, 1040–1047. [[CrossRef](#)]
56. Wang, X.; Pan, Y.; Zhu, Z.; Wu, J. Efficient degradation of rhodamine B using Fe-based metallic glass catalyst by Fenton-like process. *Chemosphere* **2014**, *117*, 638–643. [[CrossRef](#)]

57. Wang, Q.Q.; Yun, L.; Chen, M.X.; Xu, D.D.; Cui, Z.Q.; Zeng, Q.S.; Lin, P.H.; Chu, C.L.; Shen, B.L. Competitive effects of structural heterogeneity and surface chemical states on catalytic efficiency of FeSiBPCu amorphous and nanocrystalline alloys. *ACS Appl. Nano Mater.* **2019**, *2*, 214–227. [[CrossRef](#)]
58. Zhang, L.; Chen, L.Y. A review on biomedical titanium alloys: Recent progress and prospect. *Adv. Eng. Mater.* **2019**, *21*, 1801215. [[CrossRef](#)]
59. Özcan, A.; Oturan, M.A.; Oturan, N.; Şahin, Y. Removal of acid orange 7 from water by electrochemically generated Fenton's reagent. *J. Hazard. Mater.* **2009**, *163*, 1213–1220. [[CrossRef](#)]
60. Cheng, M.; Ma, W.; Li, J.; Huang, Y.; Zhao, J.; Wen, Y.X.; Xu, Y. Visible-light-assisted degradation of dye pollutants over Fe(III)-loaded resin in the presence of H₂O₂ at neutral pH values. *Environ. Sci. Technol.* **2004**, *38*, 1569–1575. [[CrossRef](#)]
61. Dai, K.; Chen, H.; Peng, T.; Ke, D.; Yi, H. Photocatalytic degradation of methyl orange in aqueous suspension of mesoporous titania nanoparticles. *Chemosphere* **2007**, *69*, 1361–1367. [[CrossRef](#)] [[PubMed](#)]
62. Devi, L.G.; Kumar, S.G.; Reddy, K.M.; Munikrishnappa, C. Photo degradation of methyl orange an azo dye by advanced Fenton process using zero valent metallic iron: Influence of various reaction parameters and its degradation mechanism. *J. Hazard. Mater.* **2009**, *164*, 459–467. [[CrossRef](#)] [[PubMed](#)]



© 2020 by the authors. Licensee MDPI, Basel, Switzerland. This article is an open access article distributed under the terms and conditions of the Creative Commons Attribution (CC BY) license (<http://creativecommons.org/licenses/by/4.0/>).